Dithered Signed-Error CMA: Robust, Computationally Efficient Blind Adaptive Equalization

Philip Schniter and C. Richard Johnson, Jr.

***Abstract*—Adaptive blind equalization has gained widespread use in communication systems that operate without training signals. In particular, the constant modulus algorithm (CMA) has become a favorite of practitioners due to its LMS-like complexity and desirable robustness properties. The desire for further reduction in computational complexity has motivated signed-error versions of CMA, which have been found to lack the robustness properties of CMA. This paper presents a simple modification of signed-error CMA, based on the judicious use of dither, that results in an algorithm with robustness properties closely resembling those of CMA. In this paper, we establish the fundamental transient and steady-state properties of dithered signed-error CMA and compare them with those of CMA.**

***Index Terms*—Adaptive equalizers, adaptive signal processing, blind equalization, constant modulus algorithm, deconvolution, dither techniques, HDTV.**

I. Introduction

THE CONSTANT modulus algorithm (CMA) [1]–[3] has gained widespread practical use as a blind adaptive equalization algorithm for digital communications systems operating over intersymbol interference channels. Modern receiver implementations often realize the advantages offered by a fractionally spaced equalizer (FSE), i.e., an equalizer operating at a rate higher than the baud rate [4] and/or processing data from multiple sensors (see, e.g., [5]). Under a set of perfect blind equalizability (PBE) conditions (listed in Section II-B), CMA-adaptation of a FSE is known to converge in mean to an equalizer setting capable of perfect symbol recovery [6], [7].

Although assumptions of ideality are convenient for the theoretical analysis of blind equalization schemes, they are unconditionally violated in physical implementations of communication systems. This fact motivates the consideration of algorithm performance under realistic (nonideal) conditions. We will use the term *robust* when referring to a blind algorithm's ability to perform "well" under violations of the PBE conditions. It has been reasoned that the widespread practical use of fractionally spaced CMA bears testament to its superior robustness properties. A sizeable body of theoretical analysis exists to support this claim [3], including, for example, studies on CMA's robustness to noise [8], channel undermodeling [9], and lack of disparity [10].

Low-cost consumer applications (e.g., HDTV) motivate blind equalization techniques requiring minimum implementation cost. Although it is noted for its LMS-like complexity, CMA may be further simplified by transforming the bulk of its update multiplications into sign operations [2]. A recent study suggests, however, that straightforward implementations of signed-error CMA (SE-CMA) do not inherit the desirable robustness properties of CMA [11]. In this paper, we present a simple modification of SE-CMA based on the judicious incorporation of controlled noise (sometimes referred to as "dither") that results in an algorithm with robustness properties closely resembling the standard (unsigned) CMA. In fact, we show that the mean behavior of dithered signed-error CMA (DSE-CMA) is *identical* to CMA under realistically achievable conditions. The anticipated drawback to this dithering is a degradation in steady-state mean-square error (MSE) performance. Hence, we derive an expression for the excess MSE (EMSE) of DSE-CMA and discuss implications on step-size and equalizer-length selection. We note in advance that the EMSE expression for DSE-CMA bears close resemblance to an analogous expression derived for CMA in [12].

The paper is partitioned as follows. Section II presents the fractionally spaced system model and reviews some fundamental properties of fractionally-spaced CMA. Section III discusses computationally-efficient blind equalization and introduces the new algorithm. The transient and steady-state properties of DSE-CMA are studied in Section IV and result in the design guidelines of Section V. Simulation results based on the Signal Processing Information Base (SPIB)[1] microwave channel models are presented in Section VI. Section VI also includes a comparison study with another robust computationally constrained implementation of CMA. For simplicity, we restrict the focus of this paper to the case of real-valued quantities. As discussed in Section VII, however, extension to the complex-valued case is straightforward.

The following is a word on notation: We use lower-case bold-face quantities (e.g., $\boldsymbol{h}$) to denote vectors and upper-case bold-face quantities (e.g., $\boldsymbol{H}$) to denote matrices. Conjugation

Manuscript received February 18. 1998; revised August 14, 1998. This work was supported in part by the National Science Foundation under Grant MIP-9509011, a Schlumberger Foundation Fellowship, and Applied Signal Technology, Inc. The associate editor coordinating the review of this paper and approving it for publication was Prof. James A. Bucklew.

The authors are with the School of Electrical Engineering, Cornell University, Ithaca, NY 14853 USA.

Publisher Item Identifier S 1053-587X(99)03688-0.

[1]The Rice University Signal Processing Information Base (SPIB) microwave channel database resides at http://spib.rice.edu/spib/microwave.html.

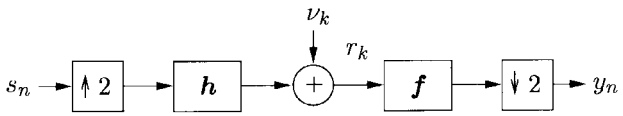

Fig. 1. $T/2$-spaced baseband communication system model.

is denoted by $(\cdot)^*$, transposition by $(\cdot)^t$, and the ℓ_2 norm by $||\cdot||$. Finally, the variable n is reserved for the baud-rate time index.

II. Fractionally Spaced CMA

A. The Fractionally Spaced System Model

In this section, we construct a received signal model based on a single-sensor receiver operating at twice the baud rate.[2] Note that an equivalent model results from the use of two sensors and that generalization to multiple sensors/oversampling is straightforward [5]. Consider a baseband communication system operating at baud interval T. A T-spaced symbol sequence $\{s_n\}$ is transmitted through a linear time-invariant and finite impulse response channel characterized by $\boldsymbol{h}$, which is a length-N_h vector of $T/2$-spaced impulse response coefficients $\{h_k\}$. In addition to intersymbol interference, the $T/2$-spaced received signal $\{r_k\}$ is also corrupted by an additive noise process $\{\nu_k\}$. The baseband receiver consists of a $T/2$-spaced linear equalizer specified by the N_f coefficients in the vector $\boldsymbol{f}$. At baud time index n, the receiver forms the symbol estimate $y_n = \boldsymbol{f}^t\boldsymbol{r}(n)$ from the previous N_f received samples, as collected in the vector $\boldsymbol{r}(n)$. Fig. 1 shows the linear system relating transmitted symbols s_n to the system outputs y_n. We assume that the source symbols s_n are drawn from a finite, zero-mean, symmetric alphabet S with variance $\sigma_s^2 := E\{|s_n|^2\}$.

Defining the $N_f \times N_q$ fractionally spaced convolution matrix $\boldsymbol{H}$, we have the equation at the bottom of the page, which allows us to write the received vector as $\boldsymbol{r}(n) = \boldsymbol{H}\boldsymbol{s}(n) + \boldsymbol{\nu}(n)$, where $\boldsymbol{\nu}(n)$ is a vector containing the previous N_f samples of the channel noise process. The baud-rate linear system relating s_n to y_n is now compactly described by the T-spaced impulse response vector $\boldsymbol{q} := \boldsymbol{H}^t\boldsymbol{f}$, so that $y_n = \boldsymbol{q}^t\boldsymbol{s}(n) + \boldsymbol{f}^t\boldsymbol{\nu}(n)$ with length-N_q source vector $\boldsymbol{s}(n) := (s_n, s_{n-1}, \cdots, s_{n-N_q+1})^t$. The structure of $\boldsymbol{H}$ implies that $N_q = \lfloor (N_h + N_f - 1)/2 \rfloor$.

[2] A more tutorial (and more complete) development of the fractionally spaced system model can be found in [3].

Perfect symbol recovery (PSR) occurs when the channel noise is absent, and when $\boldsymbol{f}$ and $\boldsymbol{H}$ are such that $y_n = as_{n-\delta}$ for all n, some fixed system delay $0 \le \delta \le N_q - 1$, and some fixed scalar a such that $|a| = 1$. The PSR system responses are characterized by $\boldsymbol{q} = a\boldsymbol{e}_\delta$ (where $\boldsymbol{e}_\delta$ denotes a vector with 1 in the δth position and zeros elsewhere). We refer to PSR-inducing equalizers as zero-forcing,[3] and denote a zero-forcing equalizer associated with system delay δ by $\boldsymbol{f}_\delta$. The goal of blind equalization can be considered the achievement (or near-achievement[4]) of PSR based only on knowledge of the system output y_n and the (marginal) statistics of the source process $\{s_n\}$.

B. The Constant Modulus Algorithm

The CMA is a stochastic gradient algorithm minimizing the Godard criterion: $J_{\rm cm} := \frac{1}{4}E\{(|y_n|^2 - \gamma)^2\}$. The positive constant γ is referred to as the dispersion constant and is chosen in accordance with the source statistics. Conceived independently in [1] and [2], the Godard criterion penalizes the dispersion of the squared output modulus $|y_n|^2$ away from γ. As an FSE update algorithm, CMA takes the form

$$\boldsymbol{f}(n+1) = \boldsymbol{f}(n) + \mu\boldsymbol{r}^*(n)\underbrace{y_n(\gamma - |y_n|^2)}_{:=\psi(y_n)} \tag{1}$$

where μ is a (small) positive step size. The function $\psi(\cdot)$ identified in (1) is referred to as the CMA error function and will appear many times throughout this paper.

The following perfect blind equalizability (PBE) conditions are known to be sufficient to guarantee that equalizers minimizing J_{cm} achieve perfect symbol recovery [3]:

- A1) full column-rank $\boldsymbol{H}$;
- A2) no additive channel noise;
- A3) sub-Gaussian source: the source's normalized kurtosis $\kappa_s := E\{|s_n|^4\}/\sigma_s^4$ must be less than that of a Gaussian process;
- A4) i.i.d. zero-mean source (circularly symmetric in the complex-valued case: $E\{s_n^2\} = 0$).

Note that A1) and A2) pertain to the channel-equalizer pair's ability to achieve PSR, whereas A3) and A4) pertain specifically to blind adaptive equalization using the Godard criterion.

[3] The terminology "zero-forcing" stems from the equalizer's ability to force the symbol estimation error to zero.

[4] When used for blind startup, i.e., those situations in which training is not present and the system error rate is too high for decision-directed (DD) techniques to function reliably, the goal of the blind algorithm may be that of reducing error rate to a level adequate for successful decision-direction.

$$\boldsymbol{H} = \begin{pmatrix} h_1 & h_0 & & & & & \\ h_3 & h_2 & h_1 & h_0 & & & \\ \vdots & \vdots & h_3 & h_2 & \ddots & h_1 & h_0 \\ h_{N_h-1} & h_{N_h-2} & \vdots & \vdots & & h_3 & h_2 \\ & & h_{N_h-1} & h_{N_h-2} & \ddots & \vdots & \vdots \\ & & & & & h_{N_h-1} & h_{N_h-2} \end{pmatrix}^t$$

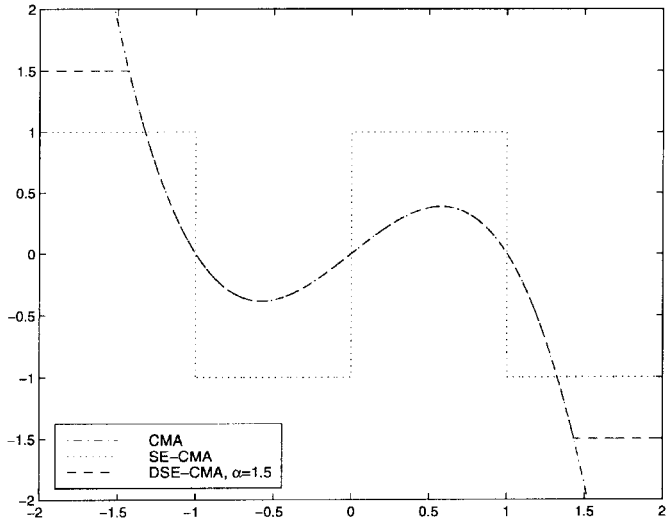

Fig. 2. CMA, SE-CMA, and DSE-CMA error functions.

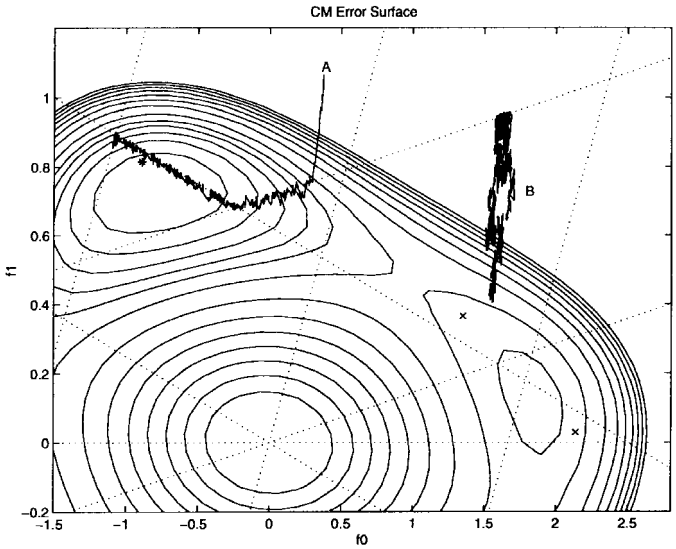

Fig. 3. SE-CMA trajectories for BPSK transmitted over noiseless channel $\boldsymbol{h} = (0.1, 0.3, 1, -0.1, 0.5, 0.2)^t$ superimposed on J_{cm} cost contours. Dotted lines delineate SE-CMA constant-gradient facets.

III. Computationally Efficient CMA

Straightforward implementations of LMS-like adaptive algorithms (such as CMA) require a multiplication between the error function and every regressor element [see update (1)]. Many practical applications benefit from eliminating these N_f regressor multiplies. Signed-error (SE) algorithms present one method for doing so, whereby only the sign of the error function is retained [13]. When a SE algorithm is combined with a power-of-two step size, it is possible to construct a multiply-free fixed-point implementation of the equalizer update algorithm. The subsections below discuss two versions of SE-CMA. (For the remainder of the paper, we restrict our focus to the case where all quantities are real valued. Extensions to the complex-valued case are discussed in Section VII.)

A. Signed-Error CMA

The real-valued SE-CMA algorithm [2] is specified as

$$\boldsymbol{f}(n+1) = \boldsymbol{f}(n) + \mu \boldsymbol{r}(n) \underbrace{\operatorname{sgn}\left(y_n(\gamma - y_n^2)\right)}_{:=\xi(y_n)} \tag{2}$$

where $\operatorname{sgn}(\cdot)$ denotes the standard signum function. Equation (2) defines the SE-CMA error function $\xi(\cdot)$ depicted in Fig. 2.

A recent investigation into SE-CMA has shown that while satisfaction of the PBE conditions and correct selection of γ ensure mean convergence to PSR, violation of A1) can severely hinder SE-CMA convergence behavior [11]. Specifically, there may exist vast yet highly suboptimal regions in equalizer space in which the expected update in (2) is zero. Fig. 3 presents an example of such behavior, in which the trajectory labeled "B" appears not to converge. (See Fig. 7 for examples of CMA trajectories under identical conditions.) Thus, while computationally efficient, SE-CMA does not inherit the desirable robustness properties of CMA. This fact motivates the search for computationally efficient blind algorithms that *do* inherit these robustness properties. The following section describes one such algorithm.

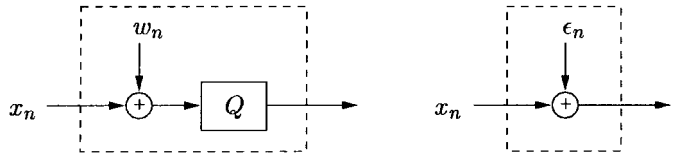

Fig. 4. Quantization noise model (right) of the dithered quantizer (left).

B. Dithered Signed-Error CMA

"*Gimme noise, noise, noise, noise* $\cdots$"—The Replacements, *Stink*, 1982.

In this section, we describe a simple modification to SE-CMA that results in an algorithm whose mean behavior closely matches that of standard (unsigned) CMA.

Viewing the SE-CMA error function as a one-bit quantizer, we might wonder whether a suitable dithering technique [14] would help to remove the unwanted behavioral artifacts caused by the sign operator.[5] Dithering refers to the addition of a random signal before quantization in an attempt to preserve the information lost in the quantization process. From an additive noise perspective, dithering is an attempt to make the so-called quantization noise (see Fig. 4) white, zero-mean, and independent of the signal being quantized. We might expect that such quantization noise could be "averaged out" by a small step-size adaptive algorithm, yielding mean behavior identical to that of its unsigned counterpart. These ideas are made precise in Section IV-B.

The real-valued dithered signed-error constant modulus algorithm (DSE-CMA) is defined [17] by the update

$$\boldsymbol{f}(n+1) = \boldsymbol{f}(n) + \mu \boldsymbol{r}(n) \underbrace{\alpha \operatorname{sgn}\left(y_n(\gamma - y_n^2) + \alpha d_n\right)}_{:=\varphi_\alpha(y_n, d_n)} \tag{3}$$

[5]The authors acknowledge a previous application of controlled noise to SE-LMS in the context of echo cancellation [15], [16]. However, both the analyzes and goals were substantially different than those in this paper.

where $\{d_n\}$ is an i.i.d. "dithering" process uniformly distributed on $(-1,1]$, both γ and α are positive constants, and $\varphi_\alpha(y_n,d_n)$ is the DSE-CMA error function. The practical selection of the dispersion constant γ and the "dither amplitude" α are discussed in Section V. It should become clear in the next section why α appears twice in (3).

IV. The Fundamental Properties of DSE-CMA

Sections IV-B to IV-D utilize an additive noise model of the dithered sign operation to characterize the transient and steady-state behaviors of DSE-CMA. Before proceeding, we present the details of this quantization noise model.

A. Quantization Noise Model of DSE-CMA

At first glance, the nonlinear sign operator in (3) appears to complicate the behavioral analysis of DSE-CMA. Fortunately, the theory of dithered quantizers allows us to subsume the sign operator by adopting a quantization-noise model of the DSE-CMA error function (see Fig. 4). Appendix A collects the key results from classical quantization theory that allow us to formulate this model.

DSE-CMA can be connected to the quantization literature with the observation that the operator $\alpha\,\mathrm{sgn}(\cdot)$ is identical to the two-level uniform quantizer $Q(\cdot)$, specified by

$$Q(x)=\begin{cases}\Delta/2, & x\geq 0\\ -\Delta/2, & x<0\end{cases} \tag{4}$$

for quantizer spacing $\Delta=2\alpha$. Furthermore, the specification that $\{d_n\}$ be uniformly distributed on $(-1,1]$ ensures that $\{\alpha d_n\}$ satisfies the requirements for a valid dither process outlined in Appendix A as long as α is selected large enough to satisfy

$$\alpha\geq|\psi(y_n)| \tag{5}$$

for relevant values of the equalizer output y_n. Recall that $\psi(\cdot)$ denotes the CMA error function, defined in (1).

Employing the model of Fig. 4, we write the DSE-CMA error function in terms of the quantization noise ϵ_n,

$$\varphi_\alpha(y_n,d_n)=\psi(y_n)+\epsilon_n \tag{6}$$

which leads to the following DSE-CMA update expression:

$$\boldsymbol{f}(n+1)=\boldsymbol{f}(n)+\mu\boldsymbol{r}(n)(\psi(y_n)+\epsilon_n). \tag{7}$$

When α and y_n satisfy (5), the properties of ϵ_n follow from (28), (29), and (31) in Appendix A. Specifically, we have that ϵ_n is an uncorrelated random process whose first moment obeys

$$E\{\epsilon_n|\psi(y_n)\}=E\{\epsilon_n\}=0 \tag{8}$$

and whose conditional second moment is given by

$$E\{\epsilon_n^2|\psi(y_n)\}=\alpha^2-\psi^2(y_n). \tag{9}$$

In (8) and (9), the expectation is taken over the dither process, thus leaving a dependence on y_n.

B. DSE-CMA Transient Behavior

The average transient behavior of DSE-CMA is completely determined by the expected DSE-CMA error function $\varphi_\alpha(y_n):=E\{\varphi_\alpha(y_n,d_n)|y_n\}$. Equations (5)–(8) indicate that $\varphi_\alpha(\cdot)$ is a "hard-limited" version of the CMA error function $\psi(\cdot)$, i.e.,

$$\varphi_\alpha(y)=\begin{cases}\alpha, & y\text{: }\psi(y)>\alpha,\\ \psi(y) & y\text{: }|\psi(y)|\leq\alpha\\ -\alpha, & y\text{: }\psi(y)<-\alpha.\end{cases} \tag{10}$$

Fig. 2 plots the various error functions $\varphi_\alpha(\cdot)$, $\psi(\cdot)$, and $\xi(\cdot)$ for comparison. In the theorems below, the implications of (10) are formalized in terms of DSE-CMA behavior over specific ranges of α.

Lemma 1: Define

$$\alpha_C:=2(\gamma/3)^{3/2}. \tag{11}$$

The choice of dither amplitude $\alpha>\alpha_C$ ensures that $\varphi_\alpha(y)=\psi(y)$ for all equalizer outputs y satisfying the output amplitude constraint $|y|\leq\psi^{-1}(\alpha)$.

Proof: By evaluating ψ at the locations where $\psi'=0$, it can be seen that the "humps" of the cubic CMA error function (see Fig. 2) occur at heights $\pm2(\gamma/3)^{3/2}$. Thus, $\psi^{-1}(\alpha)$ is unique and well-defined for $\alpha>2(\gamma/3)^{3/2}=\alpha_C$. Since (10) implies that such values of α prevent these humps from being clipped in forming the expected DSE-CMA error function, φ_α and ψ are identical over the interval $[-\psi^{-1}(\alpha),\psi^{-1}(\alpha)]$ when $\alpha>2(\gamma/3)^{3/2}$. ∎

For values $\alpha>\alpha_C$, $\psi^{-1}(\alpha)$ is determined by the unique real-valued root of the cubic polynomial $-y^3+\gamma y+\alpha$ and can be expressed as

$$\psi^{-1}(\alpha)=\tfrac{1}{6}\left(12\sqrt{81\alpha^2-12\gamma^3}-108\alpha\right)^{1/3}+2\gamma\left(12\sqrt{81\alpha^2-12\gamma^3}-108\alpha\right)^{-(1/3)}. \tag{12}$$

From (12), it can be shown that $\lim_{\alpha\to\alpha_C^+}\psi^{-1}(\alpha)=2\sqrt{\gamma/3}$.

Writing the system output as $y=\boldsymbol{r}^t\boldsymbol{f}$ for a (fixed) received vector $\boldsymbol{r}$ and arbitrary equalizer $\boldsymbol{f}$ allows the following equalizer-space interpretation of Lemma 1.

Theorem 1: Denote the set of possible received vectors by $\mathcal{R}$, and define $\mathcal{F}_\alpha$ to be the convex hull formed by the set of hyperplanes $\mathcal{B}_\alpha:=\{\boldsymbol{f}\text{: }|\boldsymbol{r}^t\boldsymbol{f}|=\psi^{-1}(\alpha)\text{ for }\boldsymbol{r}\in\mathcal{R}\}$. Then, choice of dither amplitude $\alpha>\alpha_C$ ensures that the expected DSE-CMA update is identical to the CMA update for equalizers within $\mathcal{F}_\alpha$.

Proof: Choose any two equalizers $\boldsymbol{f}_1$ and $\boldsymbol{f}_2$ that satisfy the output constraint $|\boldsymbol{r}^t\boldsymbol{f}|\leq\psi^{-1}(\alpha)$ for all $\boldsymbol{r}\in\mathcal{R}$. (Recall that $\psi^{-1}(\alpha)$ is well defined for $\alpha>\alpha_C$.) The triangle inequality implies that any convex combination of $\boldsymbol{f}_1$ and $\boldsymbol{f}_2$ also satisfies this output constraint. Lemma 1 ensures that, for $y=\boldsymbol{r}^t\boldsymbol{f}$ that satisfy the output amplitude constraint, $\varphi_\alpha(y)=\psi(y)$. Hence, the two updates are identical within $\mathcal{F}_\alpha$. ∎

For an M-ary source, the set $\mathcal{S}$ of possible source vectors $\boldsymbol{s}$ is of size M^{N_q}. Then, in the absence of channel noise, we expect at most M^{N_q} equalizer input vectors $\boldsymbol{r}=\boldsymbol{H}^t\boldsymbol{s}$. Hence, in this noiseless case, $\mathcal{F}_\alpha$ is the convex hull formed by the

finite set of M^{N_q} hyperplanes $\mathcal{B}_\alpha = \{\boldsymbol{f}\colon\ |\boldsymbol{s}^t\boldsymbol{H}\boldsymbol{f}| = \psi^{-1}(\alpha)$ for $\boldsymbol{s} \in \mathcal{S}\}$. In other words, $\mathcal{F}_\alpha$ is a polytope formed by the boundary set $\mathcal{B}_\alpha$. An illustrative example of $\mathcal{F}_\alpha$ and $\mathcal{B}_\alpha$ is provided by Fig. 6.

Next, we concern ourselves with neighborhoods of the zero-forcing (ZF) equalizers $\{\boldsymbol{f}_\delta\colon\ 0 \le \delta < N_q\}$.

Theorem 2: Define

$$\alpha_{\mathrm{ZF}} := \max_{s\in S} |\psi(s)|. \tag{13}$$

Under satisfaction of the PBE conditions, choice of dither amplitude $\alpha > \alpha_{\mathrm{ZF}}$ ensures the existence of a neighborhood around every ZF solution $\boldsymbol{f}_\delta$ within which the expected DSE-CMA update is identical to the CMA update.

Proof: When $\boldsymbol{f} = \boldsymbol{f}_\delta$, the satisfaction of the PBE conditions implies that $y_n = s_{n-\delta}$ for all s_n. In this case, (10) and the definition of α_{ZF} imply that $\psi(y_n) = \varphi_\alpha(y_n)$ for $\alpha \ge \alpha_{\mathrm{ZF}}$. In other words, $\alpha \ge \alpha_{\mathrm{ZF}}$ guarantees that the expected DSE-CMA update is identical to the CMA update *at* the zero-forcing solutions.

Now, consider an open ball $\mathcal{B}$ of radius ρ centered at $\boldsymbol{f}_\delta$. Equalizers within $\mathcal{B}$ can be parameterized as $\boldsymbol{f} = \boldsymbol{f}_\delta + \tilde{\boldsymbol{f}}$ for $||\tilde{\boldsymbol{f}}|| < \rho$. Then, there exists a finite constant K for which $|y_n - s_{n-\delta}| \le \max_{\boldsymbol{s}\in\mathcal{S}} |\boldsymbol{s}^t\boldsymbol{H}\tilde{\boldsymbol{f}}| < K\rho$. From the continuity of the polynomial function $\psi(\cdot)$, we claim the following: For any $\varepsilon := \alpha - \alpha_{\mathrm{ZF}} > 0$ and any $\boldsymbol{r} \in \mathcal{R}$, there exists a $\rho > 0$ such that $||\tilde{\boldsymbol{f}}|| < \rho$ implies $|\psi(\boldsymbol{r}^t\boldsymbol{f}) - \psi(\boldsymbol{r}^t\boldsymbol{f}_\delta)| < \varepsilon$. Applying (10), we conclude that $\psi = \varphi_\alpha$ for any equalizer within the ball $\mathcal{B}$. ■

Note that the constant α_{ZF} may be less than α_C, in which case, there would exist *isolated* "CMA-like" neighborhoods around the ZF solutions—i.e., neighborhoods not contained in any "CMA-like" convex hull.

Theorem 2 is of limited practical use since it requires satisfaction of the PBE conditions. Fortunately, the concept is easily extended to the set of "open-eye" equalizers $\mathcal{F}_{\mathrm{OE}}$. Denoting the minimum distance between any pair of adjacent symbols in S by Δ_s, we define the set $\mathcal{F}_{\mathrm{OE}}$ as[6]

$$\mathcal{F}_{\mathrm{OE}} := \{\boldsymbol{f}\colon\ \min_{\delta}\max_{\boldsymbol{r}\in\mathcal{R}} \boldsymbol{r}^t(\boldsymbol{f} - \boldsymbol{f}_\delta) < \Delta_s/2\}.$$

The corresponding set of open-eye equalizer outputs is defined by

$$Y_{\mathrm{OE}} := \{y\colon\ \min_{s\in S} |y - s| < \Delta_s/2\}.$$

For M-PAM, Y_{OE} becomes the open interval $(-s_{\max} - s_{\min}, s_{\max} + s_{\min})$ minus the set of points halfway between adjacent elements of S. Here, $s_{\min}$ and $s_{\max}$ are used to denote the minimum and maximum positive-valued elements of S, respectively.

Theorem 3: Define

$$\alpha_{\mathrm{OE}} := \max_{y\in Y_{\mathrm{OE}}} |\psi(y)|. \tag{14}$$

Choice of dither amplitude $\alpha > \alpha_{\mathrm{OE}}$ ensures the existence of a neighborhood around every open-eye equalizer $\boldsymbol{f} \in \mathcal{F}_{\mathrm{OE}}$ within which the expected DSE-CMA update is identical to the CMA update.

Proof: The proof is identical to that of Theorem 2 after replacing $s \in S$ by $y \in Y_{\mathrm{OE}}$. ■

In summary, α_C is the lower limit of α for which the convex set $\mathcal{F}_\alpha$ exists, whereas α_{ZF} and α_{OE} are the lower limits of α for which "CMA-like" local neighborhoods around the zero-forcing and open-eye equalizers exist, respectively. Table I quantifies the values of $\{\alpha_C, \alpha_{\mathrm{ZF}}, \alpha_{\mathrm{OE}}\}$ for M-PAM alphabets, and Fig. 5 illustrates their relationship to the CMA error function. Note that the difference between α_{ZF} and α_{OE} narrows as the alphabet size increases. This can be attributed to the fact that the open-eye neighborhoods shrink as the constellation becomes more dense.

TABLE I
CRITICAL VALUES OF α FOR M-PAM

M	2	4	8	16	32
α_{C}	0.38	0.81	0.90	0.92	0.93
α_{ZF}	0	0.64	0.87	1.39	1.71
α_{OE}	6	2.79	2.24	2.12	2.09

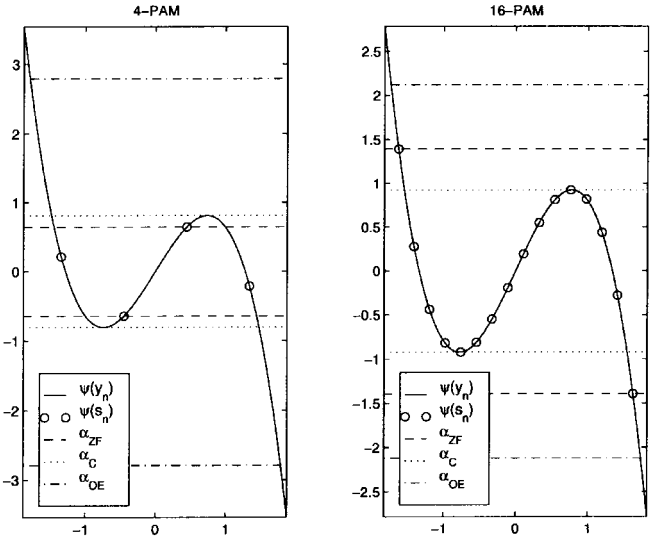

Fig. 5. CMA error function and critical values of α for 4-PAM and 16-PAM sources.

C. DSE-CMA Cost Surface

Studies of the multimodal J_{cm} cost surface give substantial insight into the transient behavior of CMA (see, e.g., [3]). Thus, we expect that an examination of J_{dse}, which is the cost stochastically minimized by DSE-CMA, should also prove worthwhile. First, however, we need to construct J_{dse}. Since we know that a gradient descent algorithm minimizing J has the general form $\boldsymbol{f}(n+1) = \boldsymbol{f}(n) - \mu\nabla_{\boldsymbol{f}}J$, we conclude from (3) that $\nabla_{\boldsymbol{f}}J_{\mathrm{dse}} = -E\{\varphi_\alpha(y_n, d_n)\boldsymbol{r}(n)\}$. It is then possible to find $J_{\mathrm{dse}}(\boldsymbol{f})$ (to within a constant) by integrating $\nabla_{\boldsymbol{f}}J_{\mathrm{dse}}$ over N_f-dimensional equalizer space.

Fig. 6 shows an illustrative example of $J_{\mathrm{dse}}(\boldsymbol{f})$ contours superimposed on $J_{\mathrm{cm}}(\boldsymbol{f})$ contours in equalizer space for

[6] We acknowledge that the definition of $\mathcal{F}_{\mathrm{OE}}$ is overly strict in that it bounds the outermost decision region from both sides. In addition, the definition of $\mathcal{F}_{\mathrm{OE}}$ only makes sense in the context of bounded inputs $\boldsymbol{r}$. Although the AWGN channel model does not ensure bounded $\boldsymbol{r}$, all practical implementations do.

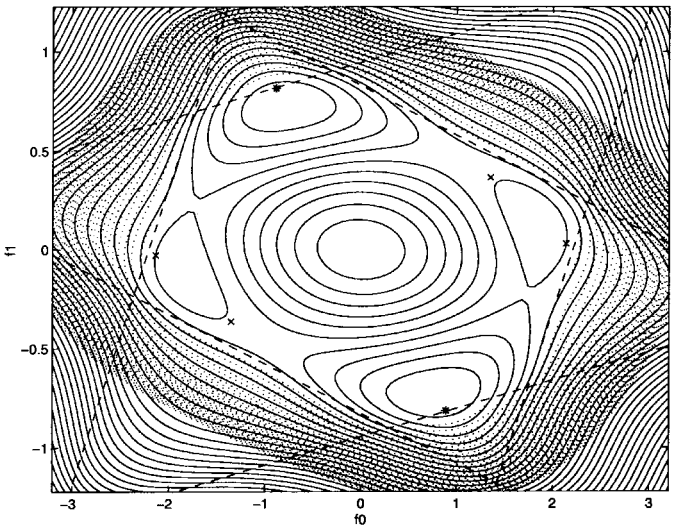

Fig. 6. Superimposed DSE-CMA (solid) and CMA (dotted) cost contours in equalizer space for BPSK, noiseless channel $\boldsymbol{h} = (0.1, 0.3, 1, -0.1, 0.5, 0.2)^t$ and $\alpha = 1$. Dashed lines show the set of hyperplanes $\mathcal{B}_\alpha$ whose convex hull $\mathcal{F}_\alpha$ ensures expected DSE-CMA behavior identical to that of CMA.

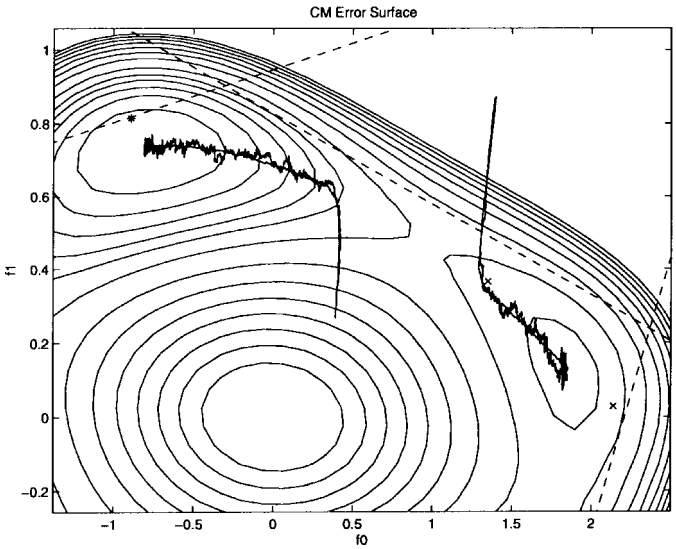

Fig. 7. Trajectories of DSE-CMA (rough) overlaid on those of CMA (smooth) for BPSK, noiseless channel $\boldsymbol{h} = (0.1, 0.3, 1, -0.1, 0.5, 0.2)^t, \mu = 5 \times 10^{-4}$, and $\alpha = 1$. Solid lines are $J_{\rm cm}$ contours, and dashed lines form the boundary set $\mathcal{B}_\alpha$.

$N_f = 2$. Note that the two sets of cost contours are identical within the convex polytope $\mathcal{F}_\alpha$ formed by the hyperplanes $\mathcal{B}_\alpha$. Outside $\mathcal{F}_\alpha$, the CMA cost contours rise much quicker than the DSE-CMA contours. This observation can be attributed to the fact that for large $||\boldsymbol{f}||$, $J_{\rm cm}(\boldsymbol{f})$ is proportional to $||\boldsymbol{f}||^4$, whereas the hard limiting on φ_α makes $J_{\rm dse}(\boldsymbol{f})$ proportional to $||\boldsymbol{f}||$. As a result, we expect that CMA exhibits much faster convergence for initializations far outside of $\mathcal{F}_\alpha$. Unlike standard SE algorithms [13], however, DSE-CMA converges *as rapidly* as its unsigned version within $\mathcal{F}_\alpha$. Fortunately, there is no need to initialize the adaptive algorithm with large $||\boldsymbol{f}||$; the "power constraint property" of CMA [8] ensures that the CMA minima lie in a hyperannulus that includes[7] $||\boldsymbol{f}|| \approx 1$ (see, e.g., Fig. 9). Initialization of DSE-CMA is discussed in Section V.

Fig. 7 shows two low-dimensional examples of a DSE-CMA trajectory overlaid on a CMA trajectory. Note that the DSE-CMA trajectories closely follow the CMA trajectories but exhibit more parameter "jitter." The effect of this parameter variation on steady-state MSE performance is quantified in the next section.

D. DSE-CMA Steady-State Behavior

The principle disadvantage of DSE-CMA concerns its steady-state behavior: The addition of dither leads to an increase in excess mean-squared error (EMSE). EMSE is typically defined as the steady-state MSE above the level attained by the fixed locally minimum MSE solution. The subsections below quantify the EMSE of DSE-CMA under the satisfaction (or near-satisfaction) of the PBE conditions.

1) Small-Error Approximation of the CMA Update: By writing the equalizer output y_n in terms of the delayed source $s_{n-\delta}$ and defining the output error $e_n := y_n - s_{n-\delta}$, the CMA error function can be written as

$$\begin{aligned}\psi(y_n) &= (\gamma - |e_n + s_{n-\delta}|^2)(e_n + s_{n-\delta}) \\ &= -e_n^3 - 3s_{n-\delta}e_n^2 - (3s_{n-\delta}^2 - \gamma)e_n + \psi(s_{n-\delta}).\end{aligned}$$

For small output error (i.e., $|e_n| \ll 1$), the error function can be approximated by

$$\psi(y_n) \approx (\gamma - 3s_{n-\delta}^2)e_n + \psi(s_{n-\delta}). \tag{15}$$

In the absence of channel noise, we can write $e_n = \boldsymbol{r}^t(n)\tilde{\boldsymbol{f}}(n)$ using the parameter error vector $\tilde{\boldsymbol{f}}(n) := \boldsymbol{f}(n) - \boldsymbol{f}_\delta$ defined relative to the zero-forcing equalizer $\boldsymbol{f}_\delta$. For adequately small $\tilde{\boldsymbol{f}}(n)$, (15) implies that the CMA error function has the approximate form

$$\psi(y_n) \approx (\gamma - 3s_{n-\delta}^2)\boldsymbol{r}^t(n)\tilde{\boldsymbol{f}}(n) + \psi(s_{n-\delta}). \tag{16}$$

Under the PBE assumptions and a reasonably small step-size, we expect asymptotically small e_n. Thus, the small-error approximation (16) can be used to characterize the steady-state behavior of DSE-CMA.

2) The Excess MSE of DSE-CMA: We define EMSE at time index n as the expected squared error above that achieved by the (local) zero-forcing solution $\boldsymbol{f}_\delta$. Since, under satisfaction of the PBE conditions, $\boldsymbol{f}_\delta$ achieves zero error

$$J_{\rm ex}(n) := E\{|\boldsymbol{r}^t(n)\tilde{\boldsymbol{f}}(n)|^2\}. \tag{17}$$

We are interested in quantifying the steady-state EMSE: $J_{\rm ex} := \lim_{n\to\infty} J_{\rm ex}(n)$. Our derivation of steady-state EMSE assumes the following:

- B1) The equalizer parameter error vector $\tilde{\boldsymbol{f}}(n)$ is statistically independent of the equalizer input $\boldsymbol{r}(n)$.
- B2) The dither amplitude α is chosen sufficiently greater than $\alpha_{\rm ZF}$ so that $\alpha > |\psi(y_n)|$ for all y_n under consideration.

[7] Assuming that the equalizer input is power-normalized, as occurs in practice.

B3) The PBE conditions A1)–A4) are satisfied to the extent that the zero-forcing solution attains near-zero error, i.e., $E\{|s_{n-\delta} - \boldsymbol{r}^t(n)\boldsymbol{f}_\delta|^2\} \approx 0$.

B4) The step size is chosen small enough for the small-error approximation (15) to hold asymptotically.

The classical assumption B1) implies that $\tilde{\boldsymbol{f}}(n)$ is independent of the source process $\{s_n\}$. Assumption B2) is needed for the results of the quantization noise model in Section IV-A to hold.

Using the facts that $\mathrm{tr}\,(A) = A$ for any scalar A and that $\mathrm{tr}\,(\tilde{\boldsymbol{f}}^t\boldsymbol{A}\tilde{\boldsymbol{f}}) = \mathrm{tr}\,(\tilde{\boldsymbol{f}}\tilde{\boldsymbol{f}}^t\boldsymbol{A})$ and $E\{\mathrm{tr}\,(\boldsymbol{A})\} = \mathrm{tr}\,(E\{\boldsymbol{A}\})$ for any matrix $\boldsymbol{A}$, the EMSE at time index n can be written

$$\begin{aligned} J_{\mathrm{ex}}(n) &= \mathrm{tr}\,(E\{\tilde{\boldsymbol{f}}(n)\tilde{\boldsymbol{f}}^t(n)\boldsymbol{r}(n)\boldsymbol{r}^t(n)\}) \\ &= \mathrm{tr}\,(E\{\tilde{\boldsymbol{f}}(n)\tilde{\boldsymbol{f}}^t(n)\}E\{\boldsymbol{r}(n)\boldsymbol{r}^t(n)\}) \end{aligned} \tag{18}$$

where the second step follows from B1). Defining the expected equalizer outer product matrix $\boldsymbol{F}(n) := E\{\tilde{\boldsymbol{f}}(n)\tilde{\boldsymbol{f}}^t(n)\}$ and the source-power-normalized regressor autocorrelation matrix $\boldsymbol{R} := (1/\sigma_s^2)E\{\boldsymbol{r}(n)\boldsymbol{r}^t(n)\}$, we can write the EMSE as

$$J_{\mathrm{ex}} = \sigma_s^2\,\mathrm{tr}\,(\boldsymbol{R}\boldsymbol{F}(n)). \tag{19}$$

Note that since $\{s_n\}$ is i.i.d. and $\boldsymbol{r}(n) = \boldsymbol{H}\boldsymbol{s}(n)$, we have $\boldsymbol{R} = \boldsymbol{H}\boldsymbol{H}^t$.

Appendix B uses the quantization noise model from Section IV-A and the error function approximation from (16) to derive the following recursion for $\boldsymbol{F}(n)$, which is valid for equalizer lengths $N_f \gg 1$:

$$\begin{aligned} \boldsymbol{F}(n+1) = \boldsymbol{F}(n) &- \mu(3-\kappa_s)\sigma_s^4(\boldsymbol{F}(n)\boldsymbol{R} + \boldsymbol{R}\boldsymbol{F}(n)) \\ &+ \mu^2\alpha^2\sigma_s^2\boldsymbol{R}. \end{aligned} \tag{20}$$

Using (19) and (20), Appendix C derives the following approximation to the steady-state EMSE of DSE-CMA:

$$J_{\mathrm{ex}} \approx \frac{\mu\alpha^2 N_f \sigma_r^2}{2(3-\kappa_s)\sigma_s^2} \tag{21}$$

where $\sigma_r^2 := E\{|r_k|^2\}$. The approximation in (21) closely matches the outcomes of experiments conducted using microwave channel models obtained from the SPIB database. The simulation results are presented in Section VI.

Equation (21) can be compared with an analogous expression for the EMSE of CMA [12]:

$$J_{\mathrm{ex|cma}} \approx \frac{\mu N_f \sigma_r^2}{2(3-\kappa_s)}\left(\frac{E\{s_n^6\}}{\sigma_s^6} - \kappa_s^2\right)\sigma_s^4. \tag{22}$$

It is apparent that the EMSE of CMA and DSE-CMA differ by the multiplicative factor

$$K_{\alpha,S} := \frac{\alpha^2}{E\{s_n^6\} - \kappa_s^2\sigma_s^6} \tag{23}$$

via $J_{\mathrm{ex}} = K_{\alpha,S}J_{\mathrm{ex|cma}}$. Note the dependence on both the dither amplitude α and the source distribution. Table II presents values of $K_{\alpha,S}$ for various M-PAM sources and particular choices of α (to be discussed in Section V-B).

V. DSE-CMA Design Guidelines

A. Selection of Dispersion Constant γ

We take the "Bussgang" approach used in [1], whereby γ is selected to ensure that the mean equalizer update is zero when perfect equalization has been achieved. From (3), (10), and the system model in Section II-A, we can write the mean update term of DSE-CMA at $\boldsymbol{f}_\delta$ (in the absence of noise) as $\mu\boldsymbol{H}E\{\boldsymbol{s}(n)\varphi_\alpha(s_{n-\delta})\}$. For an i.i.d. source, $\varphi_\alpha(s_{n-\delta})$ is independent of all but one element in $\boldsymbol{s}(n)$, namely, $s_{n-\delta}$. Hence, we require that the value of γ in φ_α be chosen so that

$$E\{s_{n-\delta}\varphi_\alpha(s_{n-\delta})\} = 0. \tag{24}$$

When $\alpha > \alpha_{\mathrm{ZF}}$, Theorem 2 ensures the existence of a neighborhood around $\boldsymbol{f}_\delta$ within which $\varphi_\alpha(y_n) = \psi(y_n)$. For such α, (24) implies that γ should be chosen as for CMA, i.e., $\gamma = E\{|s|^4\}/\sigma_s^2$ [1]. When $\alpha < \alpha_{\mathrm{ZF}}$, closed-form expressions for γ in the case of M-PAM DSE-CMA are difficult to derive. However, γ satisfying (24) for these cases can be determined numerically.

B. Selection of Dither Amplitude α

Although Section IV-D demonstrated that EMSE is proportional to α^2, Section IV-B showed that larger values of α increase the region within which DSE-CMA behaves like CMA. *The selection of dither amplitude α is therefore a design tradeoff between CMA-like robustness and steady-state MSE performance.*

Theorems 1 and 2 imply that the choice $\alpha > \max\{\alpha_C, \alpha_{\mathrm{ZF}}\}$ ensures that the zero-forcing equalizers are contained in the convex polytope $\mathcal{F}_\alpha$. Thus, under near-satisfaction of the PBE conditions, $\alpha = \max\{\alpha_C, \alpha_{\mathrm{ZF}}\}$ could be considered a useful design guideline since the CMA minima are expected to be in close proximity to the zero-forcing solutions [3]. In fact, since $\mathcal{F}_\alpha$ is convex and contains the origin, we expect that a small-norm initialization (see Section V-D) will lead to equalizer trajectories completely contained within $\mathcal{F}_\alpha$. Such a strategy is advantageous from the point of robustness.

In situations where the PBE conditions are more severely violated and CMA can do no better than "open the eye," selection of dither amplitude in the range $\max\{\alpha_C, \alpha_{\mathrm{ZF}}\} < \alpha < \max\{\alpha_C, \alpha_{\mathrm{OE}}\}$ is recommended to retain CMA-like robustness.

Table I presents these critical values of α for various M-PAM constellations. Note that the value of α_{OE} for BPSK appears unusually large because near-closed-eye operating conditions for BPSK are quite severe.

C. Selection of Step-Size μ

As in "classical" LMS theory, the selection of step size becomes a tradeoff between convergence rate and EMSE. If convergence rate in noncritical, α could be selected with robustness in mind and μ selected to meet steady-state MSE requirements.

Say that the goal was to attain the same steady-state MSE performance as CMA. Then, under satisfaction of the PBE

TABLE II
STEADY-STATE MSE RELATIVE PERFORMANCE FACTOR: $J_{\rm ex} = K_{\alpha,S} J_{\rm ex|cma}$

M-PAM	2	4	8	16	32
$K_{\alpha,S}\|_{\alpha=\max\{\alpha_C,\alpha_{\rm ZF}\}}$	-	2.9	1.6	3.3	4.8
$K_{\alpha,S}\|_{\alpha=\max\{\alpha_C,\alpha_{\rm OE}\}}$	-	34	9.8	7.6	7.2

conditions, μ should be chosen $K_{\alpha,S}^{-1}$ times that of CMA, where $K_{\alpha,S}$ was defined in (23). Table II presents values of $K_{\alpha,S}$ over the recommended range of α and can be used to predict the typical range of CMA convergence speed relative to DSE-CMA (for equal steady-state performance).

When neither convergence rate nor steady-state MSE performance can be sacrificed, Table II suggests choosing α closer to $\max\{\alpha_C, \alpha_{\rm ZF}\}$. In this case, CMA-like robustness is sacrificed instead. For such α, however, it becomes hard to predict the effects of PBE violations on the transient and steady-state performance of DSE-CMA. Loosely speaking, as α is decreased below $\max\{\alpha_C, \alpha_{\rm ZF}\}$, the performance of DSE-CMA becomes more like that of SE-CMA.

D. Initialization of DSE-CMA

The single-spike initialization [1] has become a popular initialization strategy for baud-spaced CMA, as has double-spike initialization [3], which is its $T/2$-spaced counterpart. The similarities between DSE-CMA and CMA suggest that these initialization strategies should work well for DSE-CMA as well.

In the interest of preserving CMA-like robustness, however, it is suggested the norm of the DSE-CMA initialization be kept small.[8] Under proper selection of α (i.e., $\alpha > \alpha_C$), this strategy ensures that the parameter trajectories begin within the convex region $\mathcal{F}_\alpha$ (see Fig. 9). Extending this idea, Section IV-B implies that large enough choices of α (e.g., $\alpha \approx \alpha_{\rm OE}$) ensure that the *entire* mean trajectory will stay within $\mathcal{F}_\alpha$ (and for adequately small step-sizes, the actual trajectories should closely approximate the mean trajectory). To conclude, proper choice of initialization norm and dither amplitude α will guarantee that the mean behavior of DSE-CMA never differs from that of CMA.

VI. SIMULATION RESULTS

A. Excess MSE Under PBE Conditions

Table III presents simulation results verifying the approximation of the excess MSE of DSE-CMA given in (21). The simulations were conducted using length-64 MMSE approximations of three (noiseless) SPIB microwave channels, length-62 $T/2$-spaced FSE's, and various i.i.d. M-PAM sources. In other words, PBE conditions A1) to A4) were satisfied. The step sizes were chosen so that B4) was satisfied, and the dither amplitude of $\alpha = 2$ satisfied B2). Table III gives percentage deviations from the EMSE levels predicted by (21), which were obtained by averaging the results of 2.5×10^8 iterations. Overall, the simulation results closely match our approximation (21).

[8]This is consistent with recent recommendations on the initialization of CMA in single-user applications [18].

TABLE III
$J_{\rm ex}$ DEVIATION FROM PREDICTED LEVEL FOR VARIOUS SPIB CHANNELS AND M-PAM

M-PAM	2	4	8	16	32
SPIB #2	1.3%	-0.5%	-0.5%	-0.7%	-0.5%
SPIB #3	1.2%	-0.2%	-0.6%	-1.0%	-1.0%
SPIB #4	1.4%	-0.6%	-0.6%	-0.7%	-0.7%

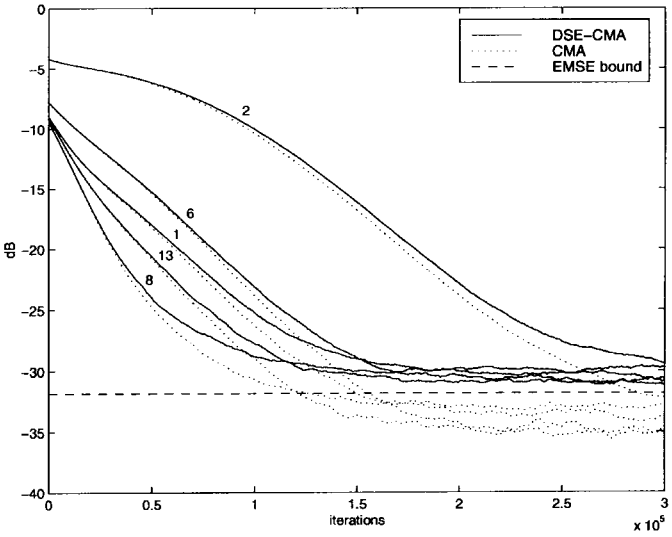

Fig. 8. Averaged MSE trajectories for DSE-CMA and CMA initialized at the same locations using 8-PAM and (normalized) SPIB channels 1, 2, 6, 8, and 13. For all simulations: SNR = 40 dB, $N_f = 32, \mu = 2 \times 10^{-5}$, and $\alpha = \alpha_{\rm OE} = 2.25$.

B. Average Transient Behavior

Throughout the paper, we have emphasized the importance of performance evaluation in realistic (nonideal) environments. It is only proper to present a comparison of DSE-CMA to CMA in this context as well. Fig. 8 shows ensemble-averaged MSE trajectories of the two algorithms operated under identical conditions and initialized at the same locations using various SPIB microwave channels. Noise levels (SNR = 40 dB) and equalizer lengths $(N_f = 32)$ were selected to represent typical applications while providing open-eye performance (for an 8-PAM source) at convergence. The following "double-spike" equalizer initialization was used in all simulations: taps 10 and 11 were set to 0.5, and all others were set to zero. Although (purposely) sub-optimal, this initialization represents a reasonable choice given the microwave channel profiles and the discussion in Section V-D. As evident in Fig. 8, the DSE-CMA trajectories track the CMA trajectories closely until the effects of EMSE take over. Fig. 8 also suggests that the EMSE approximation in (21) remains a useful guideline even under typical violations of the PBE conditions.

Although parameter trajectory comparisons are impractical with length-32 equalizers, it is easy to visualize two-tap

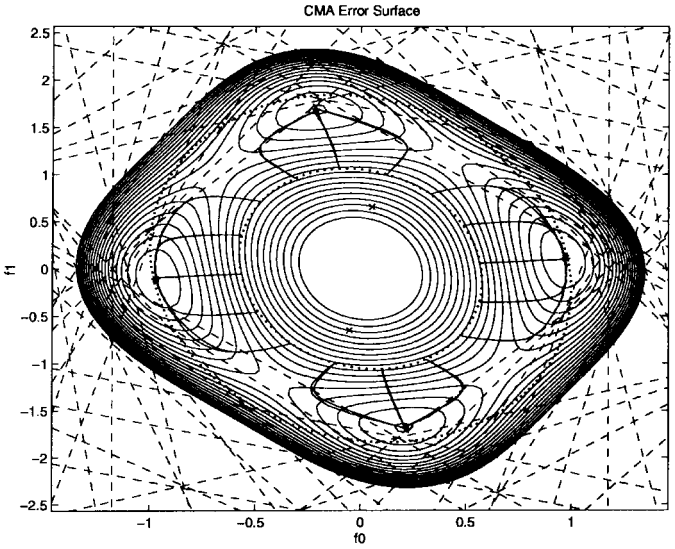

Fig. 9. Averaged DSE-CMA and CMA tap trajectories initialized at the same locations and superimposed on CMA cost contours for channel $\boldsymbol{h} = (0.1, 1, 0.5, -0.1, 0.2, 0.1)^t$, SNR = 30 dB, 4-PAM, and $\alpha = 2$. Dotted lines indicate CMA power constraint boundaries and dashed lines indicate $\mathcal{B}_\alpha$.

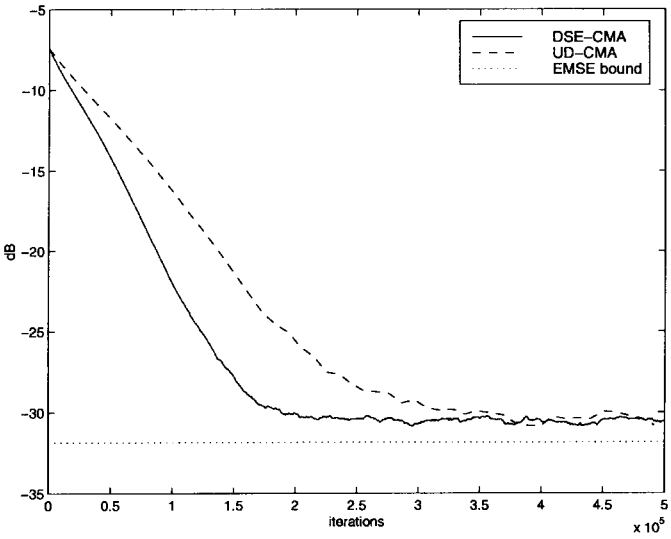

Fig. 10. Averaged MSE trajectories for DSE-CMA and update-decimated CMA initialized at the same locations using 8-PAM and SPIB channel 8. Relevant parameters: SNR = 40 dB, $N_f = 32, \alpha = \alpha_{\rm OE} = 2.25$, and update-decimation factor $D = 16$.

examples. Fig. 9 shows ensemble-averaged DSE-CMA trajectories overlaid on ensemble-averaged CMA trajectories for a noisy undermodeled channel and 4-PAM. The two trajectories in each pair correspond so closely that they are nearly indistinguishable from one another. The trajectories were initialized from various locations on the inner CMA power constraint boundary and remain, for the most part, in $\mathcal{F}_\alpha$. Note that for trajectories that cross a single boundary plane in the set $\mathcal{B}_\alpha$, the expected DSE-CMA update differs from CMA for only *one* element in the set of possible received vectors $\mathcal{R}$. In other words, loss of CMA-like behavior outside $\mathcal{F}_\alpha$ occurs gradually.

C. Comparison with Update-Decimated CMA

One popular technique used to reduce the computation requirements of CMA involves updating the equalizer every D baud samples [rather than every sample, as (1) suggests]. This is possible in situations where the channel time variations are slow with respect to the equalizer adaptation speed. As an example, fixed-site microwave applications can often tolerate update decimations of $D = 16$ and higher [19]. The fundamental drawback to these decimated algorithms is that their convergence rates decrease in proportion to D.

Since DSE-CMA and update-decimated CMA (UD-CMA) both present strategies for computationally efficient CMA-like blind adaptation, a comparison is in order. In Section V-C, we discussed how DSE-CMA step size may be selected to achieve steady-state MSE levels on par with CMA and argued that the penalty is DSE-CMA convergence rate $K_{\alpha,S}$ times slower than CMA. Although, for a given step size, UD-CMA should achieve the same steady-state performance as CMA, we expect a convergence rate that is D times slower. Taken together, we anticipate advantages in using DSE-CMA in situations where the implementation budget demands a UD-CMA decimation factor $D > K_{\alpha,S}$. (Recall that typical values of $K_{\alpha,S}$ appear in Table II.)

As verification of our claim, Fig. 10 presents ensemble-averaged MSE trajectories comparing DSE-CMA with UD-CMA for $\alpha = \alpha_{\rm OE}$ and $D = 16$. The operating environment and design quantities used were the same as those of Fig. 8, with the exception that $\mu = 2 \times 10^{-4}$ for UD-CMA. This UD-CMA step size was adjusted to equate steady-state performance, and thus, the advantage of DSE-CMA appears in the form of increased convergence rate. Checking Table II, we find that for dither amplitude $\alpha_{\rm OE}$ and an 8-PAM source, DSE-CMA is expected to "beat" UD-CMA whenever D must be selected $\geq$10.

VII. Conclusions

This paper has derived the fundamental properties of the dithered signed-error constant modulus algorithm. In summary, we have found that under proper selection of algorithmic design quantities, the expected transient behavior of DSE-CMA is *identical* to that of CMA. Although the steady-state MSE of DSE-CMA is larger than that of CMA, its value is well characterized and can be accounted for in the design procedure.

With the exception of computational complexity, the new algorithm has been designed to mimic CMA rather than "improve" on its performance. Our primary motivation for this is twofold. First, CMA is well-regarded by practitioners. It has established itself over the last 20 years as the most popular practical blind equalization algorithm, due in large part to its robustness properties [3]. It is precisely these robustness properties that we have attempted to preserve. Second, CMA has been extensively analyzed by theoreticians. The bulk of these analyses apply directly to DSE-CMA. As it is often the case that modifications of classic algorithms have disadvantages that outweigh the proposed advantages, the spirit of DSE-CMA is a computationally efficient algorithm that "leaves well enough alone."

Although we have restricted our focus to the real-valued case, a straightforward complex-valued extension of DSE-CMA is obtained by replacing the real-valued $\operatorname{sgn}(\cdot)$ in (3) with the complex-valued operator $\operatorname{csgn}(x) := \operatorname{sgn}(\operatorname{Re} x) + j \operatorname{sgn}(\operatorname{Im} x)$ and by replacing the real-valued dither process $\{d_n\}$ with the complex-valued $\{d_n^{(r)}\} + j\{d_n^{(i)}\}$. Here, $j := \sqrt{-1}$, and the processes $\{d_n^{(r)}\}$ and $\{d_n^{(i)}\}$ are real-valued, independent, and distributed identically to $\{d_n\}$. It can be shown that with minor modifications, the properties of real-valued DSE-CMA apply to its complex-valued counterpart [20]. Hence, the design guidelines of Section V apply to both the real- and complex-valued cases.

Finally, we mention a potentially useful modification to DSE-CMA. In the case of SE-LMS, the extension of the sign operator to a multilevel quantizer has been shown to yield significant performance improvements at the expense of a modest increase in computational complexity [21]. Perhaps multilevel quantization would yield similar advantages for DSE-CMA: most importantly, a reduction in EMSE.

Appendix A
Fundamental Properties of Nonsubtractively Dithered Quantizers

In this appendix, we review the key results from the theory of dithered quantizers that allow us to formulate a quantization-noise model for the DSE-CMA error function. Fig. 4 illustrates the model described below.

We define the quantization noise arising from the nonsubtractively dithered quantization of information signal x_n as

$$\epsilon_n = Q(x_n + w_n) - x_n \tag{25}$$

for a dither process $\{w_n\}$ and for $Q(\cdot)$ defined in (4). When the quantizer spacing Δ is large enough to satisfy

$$|x_n + w_n| \le \Delta \tag{26}$$

and the dither is the sum of L i.i.d. random variables uniformly distributed on $(-(\Delta/2), (\Delta/2)]$ (and statistically independent of x_n), the quantization noise has the following properties [14]:

$$E\{\epsilon_n^L | x_n\} = E\{\epsilon_n^L\} \tag{27}$$

$$E\{\epsilon_n \epsilon_m\} = E\{\epsilon_n^2\}\delta_{n-m}. \tag{28}$$

In words, (27) and (28) state that the quantization noise ϵ_n is an uncorrelated random process whose Lth moment is uncorrelated with the information signal x_n. Note that for all values of L, we have the important property that quantization noise ϵ_n is uncorrelated with the information signal x_n:

$$E\{\epsilon_n | x_n\} = E\{\epsilon_n\} = 0. \tag{29}$$

For $L = 1$, however, we have the property that the quantization noise power *is* correlated with the information signal

$$E\{\epsilon_n^2 | x_n\} \ne E\{\epsilon_n^2\}. \tag{30}$$

Although dither processes characterized by higher values of L make the quantization noise "more independent" of the information signal x_n, it is not without penalty. For one, the average noise power $E\{\epsilon_n^2\}$ increases [14], but more importantly, the class of information signals satisfying (26) for a fixed Δ shrinks. Take, for example, the case where $L = 2$ so that $\{w_n\}$ has a triangular distribution on $(-\Delta, \Delta]$. In this case, (26) is only guaranteed when $|x_n| = 0$. Worse yet, choices of $L \ge 3$ fail to meet (26) for any x_n. In other words, $\{w_n\}$ uniformly distributed on $[-(\Delta/2), (\Delta/2)]$ is the only dither process that yields a useful quantization noise model for the two-level quantizer of (4).

We will now quantify $E\{\epsilon_n^2 | x_n\}$ for uniformly distributed dither. Note that the quantization noise takes on the values $\epsilon_n \in \{-(\Delta/2) - x_n, (\Delta/2) - x_n\}$ with conditional probabilities $\{(1/2) - (x_n/\Delta), (1/2) + (x_n/\Delta)\}$, respectively. The conditional expectation then becomes

$$\begin{aligned} E\{\epsilon_n^2 | x_n\} &= \left(\frac{1}{2} - \frac{x_n}{\Delta}\right)\left(\frac{\Delta}{2} + x_n\right)^2 \\ &\quad + \left(\frac{1}{2} + \frac{x_n}{\Delta}\right)\left(\frac{\Delta}{2} - x_n\right)^2 \\ &= \frac{\Delta^2}{4} - x_n^2. \end{aligned} \tag{31}$$

Appendix B
Derivation of $\boldsymbol{F}(n+1)$

This appendix derives a recursion for the DSE-CMA parameter-error-vector expected-outer-product $\boldsymbol{F}(n) := E\{\tilde{\boldsymbol{f}}(n)\tilde{\boldsymbol{f}}^t(n)\}$. We assume that B1)–B4), which were stated in Section IV-D2, hold. In the sequel, the notation $[a_{i,j}]$ will be used to denote a matrix whose (i,j)th entry is specified by $a_{i,j}$.

Under B2), subtracting $\boldsymbol{f}_\delta$ from both sides of (7) yields $\tilde{\boldsymbol{f}}(n+1) = \tilde{\boldsymbol{f}}(n) + \mu \boldsymbol{r}(n)(\psi(y_n) + \epsilon_n)$. Thus, the expectation of the outer product of $\tilde{\boldsymbol{f}}(n+1)$ is

$$\begin{aligned} \boldsymbol{F}(n+1) &= \boldsymbol{F}(n) + \mu E\{(\psi(y_n) + \epsilon_n)\tilde{\boldsymbol{f}}(n)\boldsymbol{r}^t(n)\} \\ &\quad + \mu E\{(\psi(y_n) + \epsilon_n)\boldsymbol{r}(n)\tilde{\boldsymbol{f}}^t(n)\} \\ &\quad + \mu^2 E\{\boldsymbol{r}(n)\boldsymbol{r}^t(n)\psi^2(y_n)\} \\ &\quad + 2\mu^2 E\{\boldsymbol{r}(n)\boldsymbol{r}^t(n)\psi(y_n)\epsilon_n\} \\ &\quad + \mu^2 E\{\boldsymbol{r}(n)\boldsymbol{r}^t(n)\epsilon_n^2\}. \end{aligned}$$

The quantization noise properties (8) and (9) can be applied to simplify the previous expression.

$$\begin{aligned} \boldsymbol{F}(n+1) &= \boldsymbol{F}(n) + \mu E\{\psi(y_n)\tilde{\boldsymbol{f}}(n)\boldsymbol{r}^t(n)\} \\ &\quad + \mu E\{\psi(y_n)\boldsymbol{r}(n)\tilde{\boldsymbol{f}}^t(n)\} \\ &\quad + \mu^2\alpha^2 E\{\boldsymbol{r}(n)\boldsymbol{r}^t(n)\}. \end{aligned}$$

Applying the small-error approximation (16), the outer product recursion is well described, for small $\tilde{\boldsymbol{f}}(n)$, by

$$\begin{aligned} \boldsymbol{F}(n+1) &= \boldsymbol{F}(n) + \mu E\{(\gamma - 3s_{n-\delta}^2)\tilde{\boldsymbol{f}}(n)\tilde{\boldsymbol{f}}^t(n)\boldsymbol{r}(n)\boldsymbol{r}^t(n)\} \\ &\quad + \mu E\{(\gamma - 3s_{n-\delta}^2)\boldsymbol{r}(n)\boldsymbol{r}^t(n)\tilde{\boldsymbol{f}}(n)\tilde{\boldsymbol{f}}^t(n)\} \\ &\quad + \mu E\{\psi(s_{n-\delta})\tilde{\boldsymbol{f}}(n)\boldsymbol{r}^t(n)\} \\ &\quad + \mu E\{\psi(s_{n-\delta})\boldsymbol{r}(n)\tilde{\boldsymbol{f}}^t(n)\} \\ &\quad + \mu^2\alpha^2 E\{\boldsymbol{r}(n)\boldsymbol{r}^t(n)\}. \end{aligned} \tag{32}$$

The individual terms in (32) are successively analyzed below.

The second and third terms in (32) are transposes of one another. For now, we concentrate on the first of the pair, for which we can use B1) and the fact that $E\{\boldsymbol{r}(n)\boldsymbol{r}^t(n)\} = \sigma_s^2\boldsymbol{H}\boldsymbol{H}^t = \sigma_s^2\boldsymbol{R}$ to write

$$E\{(\gamma - 3s_{n-\delta}^2)\tilde{\boldsymbol{f}}(n)\tilde{\boldsymbol{f}}^t(n)\boldsymbol{r}(n)\boldsymbol{r}^t(n)\} = \boldsymbol{F}(n)(\sigma_s^2\gamma\boldsymbol{R} - 3E\{s_{n-\delta}^2\boldsymbol{r}(n)\boldsymbol{r}^t(n)\}).$$

Since $E\{s_{n-\delta}^2\boldsymbol{r}(n)\boldsymbol{r}^t(n)\} = \boldsymbol{H}E\{s_{n-\delta}^2\boldsymbol{s}(n)\boldsymbol{s}^t(n)\}\boldsymbol{H}^t$, we define the matrix $[a_{i,j}] = E\{s_{n-\delta}^2\boldsymbol{s}(n)\boldsymbol{s}^t(n)\}$ with elements

$$a_{i,j} = E\{s_{n-\delta}^2 s_{n-i}s_{n-j}\} = \begin{cases} 0, & i \neq j \\ \sigma_s^4, & i = j \neq \delta \\ E\{s_{n-\delta}^4\}, & i = j = \delta. \end{cases}$$

Then in matrix notation, $[a_{i,j}] = \sigma_s^4\boldsymbol{I} + (E\{s_{n-\delta}^4\} - \sigma_s^4)\boldsymbol{e}_\delta\boldsymbol{e}_\delta^t$ (where $\boldsymbol{e}_\delta$ is a vector with a one in the δth position and zeros elsewhere). Incorporating the definition of κ_s from A3), we conclude that

$$E\{s_{n-\delta}^2\boldsymbol{r}(n)\boldsymbol{r}^t(n)\} = \sigma_s^4\boldsymbol{H}\boldsymbol{H}^t + \sigma_s^4(\kappa_s - 1)\boldsymbol{H}\boldsymbol{e}_\delta\boldsymbol{e}_\delta^t\boldsymbol{H}^t.$$

For long equalizers (i.e., $N_f \gg 1$), the second term in the preceding equation is dominated by the first so that we can approximate

$$E\{s_{n-\delta}^2\boldsymbol{r}(n)\boldsymbol{r}^t(n)\} \approx \sigma_s^4\boldsymbol{H}\boldsymbol{H}^t = \sigma_s^4\boldsymbol{R}.$$

Finally, since $\gamma = \sigma_s^2\kappa_s$, these approximations yield

$$\mu E\{(\gamma - 3s_{n-\delta}^2)\tilde{\boldsymbol{f}}(n)\tilde{\boldsymbol{f}}^t(n)\boldsymbol{r}(n)\boldsymbol{r}^t(n)\} + \mu E\{(\gamma - 3s_{n-\delta}^2)\boldsymbol{r}(n)\boldsymbol{r}^t(n)\tilde{\boldsymbol{f}}(n)\tilde{\boldsymbol{f}}^t(n)\} = -\mu(3 - \kappa_s)\sigma_s^4(\boldsymbol{F}(n)\boldsymbol{R} + \boldsymbol{R}\boldsymbol{F}(n)).$$

As for the fourth and fifth terms of (32), notice that B1) implies $E\{\psi(s_{n-\delta})\tilde{\boldsymbol{f}}(n)\boldsymbol{r}^t(n)\} = E\{\tilde{\boldsymbol{f}}(n)\}E\{\psi(s_{n-\delta})\boldsymbol{s}^t(n)\}\boldsymbol{H}^t$. As we know from Section V-A, the dispersion constant is selected to force $E\{\psi(s_{n-\delta})\boldsymbol{s}^t(n)\} = 0$. Thus, the fourth and fifth terms of (32) vanish.

Rewriting the final term of (32), the approximated outer product recursion (valid for small $\tilde{\boldsymbol{f}}(n)$ and $N_f \gg 1$) becomes

$$\boldsymbol{F}(n+1) = \boldsymbol{F}(n) - \mu(3 - \kappa_s)\sigma_s^4(\boldsymbol{F}(n)\boldsymbol{R} + \boldsymbol{R}\boldsymbol{F}(n)) + \mu^2\alpha^2\sigma_s^2\boldsymbol{R}.$$

APPENDIX C
DERIVATION OF J_{ex}

In this appendix, we use (20) to determine an expression for the steady-state EMSE achieved by DSE-CMA. A similarity transformation of the symmetric Toeplitz matrix $\boldsymbol{R}$ is employed to simplify the derivation $\boldsymbol{R} = \boldsymbol{Q}\boldsymbol{\Lambda}\boldsymbol{Q}^t$, where the matrix $\boldsymbol{\Lambda}$ is diagonal, and the matrix $\boldsymbol{Q}$ is orthogonal. Applying this transformation to $\boldsymbol{F}(n)$ yields $\boldsymbol{F}(n) = \boldsymbol{Q}\boldsymbol{X}(n)\boldsymbol{Q}^t$, where $\boldsymbol{X}(n)$ is, in general, *not* diagonal. Using the properties of the trace operator and the fact that $\boldsymbol{Q}^t\boldsymbol{Q} = \boldsymbol{I}$, we can express the EMSE from (19) in terms of the transformed variables

$$J_{\text{ex}}(n) = \sigma_s^2 \operatorname{tr}(\boldsymbol{\Lambda}\boldsymbol{X}(n)).$$

The diagonal nature of $\boldsymbol{\Lambda}$ implies $J_{\text{ex}}(n) = \sigma_s^2\,\Sigma_i\,\lambda_i x_i(n)$, where λ_i and $x_i(n)$ represent the ith diagonal elements of $\boldsymbol{\Lambda}$ and $\boldsymbol{X}(n)$, respectively.

The similarity transformation can be applied to (20) to obtain a recursion in terms of $\boldsymbol{X}(n)$.

$$\boldsymbol{X}(n+1) = \boldsymbol{X}(n) - \mu(3 - \kappa_s)\sigma_s^4(\boldsymbol{X}(n)\boldsymbol{\Lambda} + \boldsymbol{\Lambda}\boldsymbol{X}(n)) + \mu^2\alpha^2\sigma_s^2\boldsymbol{\Lambda}.$$

For the characterization of J_{ex}, we are interested in only the steady-state values of the diagonal elements $x_i(n)$. In terms of the ith element

$$x_i(n+1) = x_i(n) - 2\mu(3 - \kappa_s)\sigma_s^4 x_i(n)\lambda_i + \mu^2\alpha^2\sigma_s^2\lambda_i.$$

Because $|x_i(n+1) - x_i(n)| \to 0$ as $n \to \infty$, the limit of the previous equation becomes

$$2\mu(3 - \kappa_s)\sigma_s^4 x_i\lambda_i = \mu^2\alpha^2\sigma_s^2\lambda_i$$

where we have introduced the shorthand notation $x_i = \lim_{n\to\infty} x_i(n)$. We can now sum over i to obtain

$$J_{\text{ex}} = \frac{\mu\alpha^2}{2(3 - \kappa_s)}\sum_i \lambda_i.$$

Using the fact that $\Sigma_i\,\lambda_i = \operatorname{tr}(\boldsymbol{R}) = E\{\boldsymbol{r}^t(n)\boldsymbol{r}(n)\} = N_f\sigma_r^2/\sigma_s^2$, we finalize our approximation for J_{ex}, which is the asymptotic EMSE of DSE-CMA:

$$J_{\text{ex}} = \frac{\mu\alpha^2 N_f\sigma_r^2}{2(3 - \kappa_s)\sigma_s^2}.$$

An alternate, although useful, form for J_{ex} can be obtained using the relation $\Sigma_i\,\lambda_i = \operatorname{tr}(\boldsymbol{H}\boldsymbol{H}^t) = (N_f/2)||\boldsymbol{h}||^2$ for even N_f:

$$J_{\text{ex}} = \frac{\mu\alpha^2 N_f||\boldsymbol{h}||^2}{4(3 - \kappa_s)}.$$

REFERENCES

[1] D. N. Godard, "Self-recovering equalization and carrier tracking in two-dimensional data communication systems," *IEEE Trans. Commun.*, vol. COMM-28, pp. 1867–1875, Nov. 1980.

[2] J. R. Treichler and B. G. Agee, "A new approach to multipath correction of constant modulus signals," *IEEE Trans. Acoust., Speech, Signal Processing*, vol. ASSP-31, pp. 459–472, Apr. 1983.

[3] C. R. Johnson, Jr. *et al*., "Blind equalization using the constant modulus criterion: A review," *Proc. IEEE* (Special Issue on Blind System Identification and Estimation), vol. 86, pp. 1927–1950, Oct. 1998.

[4] R. D. Gitlin, J. F. Hayes, and S. B. Weinstein, *Data Communications Principles*. New York: Plenum, 1992.

[5] E. Moulines, P. Duhamel, J. Cardoso, and S. Mayrargue, "Subspace methods for blind identification of multichannel FIR filters," *IEEE Trans. Signal Processing*, vol. 43, pp. 516–525, Feb. 1995.

[6] Y. Li and Z. Ding, "Global convergence of fractionally spaced Godard (CMA) adaptive equalizers," *IEEE Trans. Signal Processing*, vol. 44, pp. 818–826, Apr. 1996.

[7] I. Fijalkow, F. Lopez de Victoria, and C. R. Johnson, Jr., "Adaptive fractionally spaced blind equalization," in *Proc. IEEE Signal Process. Workshop*, Yosemite Nat. Park, CA, Oct. 1994, pp. 257–260.

[8] H. H. Zeng, L. Tong, and C. R. Johnson, Jr., "Relationships between the constant modulus and Wiener receivers," *IEEE Trans. Inform. Theory*, vol. 44, pp. 1523–1538, July 1998.

[9] T. J. Endres, B. D. O. Anderson, C. R. Johnson, Jr., and M. Green, "Robustness to fractionally-spaced equalizer length using the constant modulus criterion," *IEEE Trans. Signal Processing*, vol. 47, pp. 544–549, Feb. 1999.
[10] I. Fijalkow, A. Touzni, and J. R. Treichler, "Fractionally spaced equalization using CMA: Robustness to channel noise and lack of disparity," *IEEE Trans. Signal Processing*, vol. 45, pp. 56–66, Jan. 1997.
[11] D. R. Brown, P. Schniter, and C. R. Johnson, Jr., "Computationally efficient blind equalization," in *Proc. 35th Allerton Conf. Commun., Contr., Comput.*, Monticello, IL, Sept. 1997, pp. 54–63.
[12] I. Fijalkow, C. E. Manlove, and C. R. Johnson, Jr., "Adaptive fractionally spaced blind CMA equalization: Excess MSE," *IEEE Trans. Signal Processing*, vol. 46, pp. 227–231, Jan. 1998.
[13] O. Macchi, *Adaptive Processing*. New York: Wiley, 1995.
[14] R. M. Gray and T. G. Stockham, Jr., "Dithered quantizers," *IEEE Trans. Inform. Theory*, vol. 39, pp. 805–812, May 1993.
[15] N. Holte and S. Stueflotten, "A new digital echo canceller for two-wire subscriber lines," *IEEE Trans. Commun.*, vol. COMM-29, pp. 1573–1580, Nov. 1981.
[16] M. Bonnet and O. Macchi, "An echo canceller having reduced size word taps and using the sign algorithm with extra controlled noise," in *Proc. Int. Conf. Acoust., Speech, Signal Process.*, San Diego, CA, Mar. 1984, pp. 30.2.1–30.2.4.
[17] P. Schniter and C. R. Johnson, Jr., "The dithered signed-error constant modulus algorithm," in *Proc. Int. Conf. Acoust., Speech, Signal Process.*, Seattle, WA, May 1998, pp. 3353–3356.
[18] W. Chung and C. R. Johnson, Jr., "Characterization of the regions of convergence of CMA adaptive blind fractionally spaced equalizers," in *Proc. Asilomar Conf. Signals, Syst., Comput.*, Pacific Grove, CA, Nov. 1998.
[19] J. R. Treichler,, M. G. Larimore, and J. C. Harp, "Practical blind demodulators for high-order QAM signals," *Proc. IEEE*, Special Issue on Blind System Identification and Equalization, vol. 86, pp. 1907–1926, Oct. 1998.
[20] P. Schniter and C. R. Johnson, Jr., "Dithered signed-error CMA: The complex-valued case," in *Proc. Asilomar Conf. Signals, Syst., Comput.*, Pacific Grove, CA, Nov. 1998.
[21] D. L. Duttweiler, "Adaptive filter performance with nonlinearities in the correlation multiplier," *IEEE Trans. Acoust., Speech, Signal Processing*, vol. ASSP-30, pp. 578–586, Aug. 1982.

Philip Schniter was born in Evanston, IL, in 1970. He received the B.S. and M.S. degrees in electrical and computer engineering from the University of Illinois, Urbana-Champaign, in 1992 and 1993, respectively. Since 1996, he has been pursuing the Ph.D. degree in electrical engineering at Cornell University, Ithaca, NY, where he has received the 1998 Schlumberger Fellowship and the 1998–1999 Intel Foundation Fellowship.

From 1993 to 1996, he was employed by Tektronix, Inc., Beaverton, OR, as a Systems Engineer, where he worked on signal processing aspects of video and communications instrumentation design, including algorithms, software, and hardware architectures. His research interest is signal processing for communication systems, especially blind adaptive equalization.

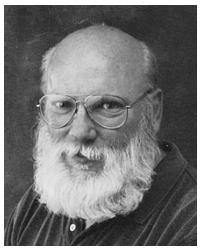

C. Richard Johnson, Jr. was born in Macon, GA, in 1950. He received the Ph.D. degree in electrical engineering with minors in engineering-economic systems and art history from Stanford University, Stanford, CA, in 1977.

He is currently a Professor of electrical engineering and a Member of the Graduate Field of Applied Mathematics at Cornell University, Ithaca, NY. His research in adaptive parameter estimation theory with applications in signal processing, communication systems, system identification, and digital control has been supported by the National Science Foundation, the Engineering Foundation, the National Aeronautics and Space Administration, Tellabs Research Laboratory, MOOG Technology Center, United Technologies Research Center, Lucent Technologies, and Applied Signal Technology. His current research interest is in adaptive parameter estimation theory useful in applications of digital signal processing to telecommunication systems. His principal focus in the 1990's has been blind linear equalization for intersymbol interference removal from received QAM sources.